Upper crustal azimuthal anisotropy across the contiguous US determined by Rayleigh wave ellipticity

Fan-Chi Lin[1] & Brandon Schmandt[2]

1. Department of Geology and Geophysics, The University of Utah, Salt Lake City, UT 84112, USA (**FanChi.Lin@utah.edu)**

2. Department of Earth and Planetary Science, The University of New Mexico, Albuquerque, NM 87131, USA

Abstract

Constraints on upper crustal seismic anisotropy provide insight into the local stress orientation and structural fabric, but such constraints are scarce except in areas with dense recordings of local seismicity. We investigate directionally dependent Rayleigh wave ellipticity, or Rayleigh wave H/V (horizontal to vertical) amplitude ratios, between 8-20 s period across USArray to infer azimuthal anisotropy in the upper crust across the contiguous US. To determine the H/V ratios, we use all available multicomponent ambient noise cross correlations between all USArray stations operating between 2007 and 2013. In many locations, the observed H/V ratios are clearly back azimuth dependent with a 180° degree periodicity, which allows the fast directions and amplitudes of upper crustal anisotropy to be determined. The observed patterns of anisotropy correlate well with both near-surface geological features (e.g. the Inter Mountain Seismic Belt and Appalachian-Ouachita collision belt) and a previous stress model.

1. Introduction

Structural fabric and stress-induced microcrack alignment are often considered as the primary causes for upper crustal anisotropy (Boness and Zoback, 2006; Crampin 1978; Kern & Wenk 1990; Aster & Shearer, 1992; Gerst & Shear, 2004; Sherrington et al., 2004; Yang et al., 2011). Traditional seismic methods often use shear wave splitting from local earthquakes to investigate shallow crustal anisotropy (Crampin & Lovell, 1991; Savage, 1999). This approach is limited by the seismic source distribution and is not applicable in areas where seismicity is infrequent. The recent development of ambient noise tomography and the availability of passive data from industrial-type dense arrays provide an alternative way to study shallow crustal structure using high frequency (~0.3-4 Hz) surface waves extracted from ambient noise (Lin et al., 2013; Mordret et al., 2013). Such an approach is limited to very local scales and continuous mapping of upper crustal anisotropy on regional or continental scales remains a challenge.

Recent studies on Rayleigh wave ellipticity provide a new approach to studying shallow earth structure across larger scales using broadband arrays (Yano et al., 2009; Lin et al.,2012; Tanimoto and Rivera, 2008; Tanimoto et al., 2013; Lin et al., 2012; Lin et al., 2014). Rayleigh wave ellipticity, described by the Rayleigh wave horizontal to vertical amplitude ratio (H/V ratio), is a site property with significant shallow sensitivity (Figure 1; Boore and Toksöz, 1969; Tanimoto and Rivera, 2008). Different from the traditional noise spectral H/V ratio (Bonnefoy-Claudet et al., 2006), the Rayleigh wave H/V ratio can be theoretically determined for a 1D earth model using the Rayleigh wave radial and vertical eigenfunctions (Tanimoto and Rivera, 2008). Studying Rayleigh wave H/V ratios

using either earthquake signals or ambient noise cross correlations has led to improved crustal models in both southern California and other parts of the western US (Lin et al., 2012; Lin et al., 2013; Tanimoto et al., 2013). Throughout this manuscript, we sometimes refer to the Rayleigh wave H/V ratio as 'the H/V ratio' for conciseness, but the term should not be confused with the traditional noise spectral H/V ratio.

In this study, we explore the possibility of studying upper crustal anisotropy across the contiguous US using the directionally dependent Rayleigh wave H/V ratio measurements. Similar to Rayleigh wave phase velocities, Rayleigh wave H/V ratios are sensitive to azimuthal anisotropy of shear wave velocity (Tanimoto et al., 2008), and like isotropic H/V ratios, such sensitivity is extremely shallow, which allows upper crustal anisotropy to be constrained. Here, following our previous Rayleigh wave H/V ratio study with multicomponent ambient noise cross correlations in the western US (Lin et al., 2014), we first expand our data coverage to include most of the contiguous US and then analyze the azimuthal dependence of Rayleigh wave H/V ratio measurements. Clear anisotropy signals are identified based on observations of 180° periodicity in the H/V ratio. The resulting map of inferred upper crustal anisotropy correlates well with known geological structures and the stress field in North America previously inferred from independent measurements (Heidbach et al., 2010).

2. Data and Results

We closely follow the method described by Lin et al. (2014) to obtain 8 to 20 s Rayleigh wave H/V ratio measurements across USArray. First, all available three-component ambient noise records between 1 January 2007 and 31 December 2013 are used to

compute ZZ, ZR, RZ, and RR (Z and R represent vertical and radial components, respectively) noise cross correlations between all stations (Bensen et al., 2007; Lin et al., 2008). Simultaneous temporal and spectral normalization of each component's noise time series is performed prior to cross correlation to ensure the amplitude ratio information between different components is not lost (Lin et al., 2014). For each station pair, the amplitude ratios between different component cross correlations are then used to determine Rayleigh wave H/V ratios at the two station locations, considering one station as a virtual source and the other as a receiver. The Rayleigh wave H/V ratios derived from different virtual sources but at the same receiver location are averaged to obtain the isotropic H/V ratio. Back azimuth dependence of the H/V ratio at the receiver location is identified by binning the virtual sources in 20° increments, where the back-azimuth direction of each measurement is determined by the great-circle-path connecting the virtual source to the receiver. Examples of raw directionally dependent H/V ratio measurements before averaging and stacking can be found in Figure S1 in the Supporting Information.

Figure 1 summarizes the 10 and 16 s period Rayleigh wave isotropic H/V ratios observed across USArray. Here a 0.5° Gaussian smoothing is applied to interpolate the result from station locations to a 0.2° × 0.2° grid (Figure 1a,c). At these periods, the H/V ratios are most sensitive to upper crustal structure. High H/V ratios typically represent strong positive velocity gradients in the upper crust, such as a sedimentary basins overlying relatively high-velocity bedrock. Low H/V ratios typically represent weak velocity gradients in the upper crust, which are common where high-velocity bedrock is reached at very shallow depths or outcrops at the surface. In the western US, the results are

consistent with our prior study (Lin et al., 2014), with high H/V ratios observed in major sedimentary basins and low H/V ratios observed in major mountain ranges. In the east, extremely high H/V ratios are observed in the Mississippi Embayment where thick sediments are present (Laske and Masters, 1997). Slightly higher than average H/V ratios are also observed in the mid-continental rift, likely related to the shallow sediments in the failed rift system (Hinze et al., 1992; Shen et al., 2013). Low H/V ratios are observed in areas where deeply exhumed bedrock outcrops at the surface including the Laurentian Highlands, the Ouachita-Ozark Interior Highlands, and the Appalachian Highlands. A 3D inversion integrating other types of surface wave dispersion measurements (e.g., Lin et al., 2012; Lin et al., 2014) will be the subject of future studies. Here, we focus on investigation of azimuthal anisotropy in H/V ratios extracted from ambient noise.

For each station and period, we remove the isotropic H/V ratio from each H/V ratio measurement to isolate directionally dependent variations. For each location all measurements from stations within 100 km are used in order to boost the signal-to-noise ratio. Measurements within each 20° back azimuth bin are summarized to calculate the averaged H/V ratio perturbation and its uncertainty. Figure 2 shows the observed directionally dependent H/V ratio variations for the 10 and 16 s period Rayleigh waves at three distinct geological locations. In northern Utah and southwestern Virginia clear 180° periodicity is the H/V ratio is observed, which is a signature of an azimuthally anisotropic medium (Smith & Dahlen 1973). Both stations exhibit anisotropic H/V ratios with peak-to-peak amplitudes of ~7%. In contrast, the third example station located southern Nebraska does not exhibit a robust anisotropic signal, which suggests that the upper crustal structure in this location within the Interior Plains Province is mostly isotropic.

120

121 Wherever a clear anisotropy pattern is observed, the directionally dependent H/V ratio
122 measurements allow us to determine the high and low H/V ratio directions and anisotropy
123 amplitude based on least squares fitting. Previous azimuthal anisotropy studies across
124 USArray based on Rayleigh wave phase velocity measurements suggest that anisotropy
125 in the middle/lower crust is normally smaller than 2% (Lin et al., 2009; Lin et al., 2011).
126 Regional upper crustal anisotropy studies, on the other hand, suggest that the uppermost
127 crust can be significantly anisotropic with amplitudes larger than 10% in some cases (Lin
128 et al., 2013; Crampin, 1994). These earlier observations suggest that the strong anisotropy
129 signals (Figure 2a,c,d,f) observed for the H/V ratios are most likely related to anisotropic
130 structure in the uppermost crust.

131

132 We assume the strength of azimuthal anisotropy amplitude decreases rapidly with depth
133 and the observed H/V ratio anisotropy is mostly related to the azimuthal anisotropy in the
134 top ~3 km. Figure 3 summarizes the observed 10 and 16 s period Rayleigh wave H/V
135 ratio azimuthal anisotropy and the inferred upper crustal fast directions across the
136 contiguous US. Here, we remove all locations with more than a 120° back-azimuth gap in
137 the H/V ratio measurements to retain only the most robust measurements. This, however,
138 also removes all locations near the edges of USArray. Overall, the observed anisotropy
139 patterns are very similar for the two periods, consistent with the shallow anisotropy
140 assumption, as both periods are strongly sensitive to the uppermost crustal structure
141 (Figure 1b,d).

142

143 **3. Discussion**

144 In the western US, anisotropy with amplitude >2% is observed in most geological
145 provinces except the Colorado Plateau. In the Great Basin, persistent north-south fast
146 directions are observed at the 16 s period, which are likely related to the north-south
147 basin and range alignment and the principal east-west extensional stress (Flesch et al.,
148 2000). The anisotropy is particularly strong on the eastern edge of the Great Basin, where
149 higher than 8% anisotropy is observed in both the 10 and 16 s periods and the north-south
150 fast directions are aligned with the Intermountain Seismic Belt (Smith and Sbar, 1974).
151 Strong anisotropy is also observed in the Northern and Southern Rockies where fast
152 directions are subparallel to the Rocky Mountain Front.
153
154 In the eastern US, a striking correlation is observed between the anisotropy pattern and
155 the inferred Precambrian Rift Margins that parallel the Appalachian-Ouachita ancient
156 collision belt (Whitmeyer & Karlstrom, 2007). Strong anisotropy (>6%) is observed in
157 both the 10 and 16 s periods with fast directions well aligned with the strike of major
158 mountain ranges. Intriguingly, the anisotropy fast directions rotate ~90° at both southern
159 Alabama and southeastern Oklahoma, closely following the inferred orientation change
160 of the Precambrian Rift Margin (Whitmeyer & Karlstrom, 2007). Different from the
161 isotropic H/V ratio pattern observed (Figure 1), the anisotropy pattern follows the
162 Precambrian Rift Margin across the Mississippi embayment and hence it is not simply
163 correlated with thick sedimentary deposits. Away from the ancient rift margins, weak to
164 negligible anisotropy is observed across the cratonic interior except in the area of the
165 Midcontinental Rift. Intermediate amplitude anisotropy (~4%) is observed at the 10 s
166 period near the Midcontinental Rift in Iowa and Minnessota with the fast direction
167 subparallel to the rift system. At the same location, negligible anisotropy is observed at

168 the 16 s period, however, suggesting the anisotropic structure associated with the
169 Midcontinental Rift system may change significantly over small changes in depth.
170
171 Distinguishing between the effects of stress induced microcrack alignment and structural
172 fabric (e.g., foliation) on observations of H/V ratio anisotropy can be difficult. In
173 particular, major geological features often align with the principal stress direction (such
174 as the Basin and Range Province) and the gravitational potential energy variations
175 associated with major geological features can also induce regional deviatoric stress
176 (Jones et al., 1996; Flesch et al., 2000). When the stress field is not hydrostatic,
177 microcracks aligned with the maximum compressive principal axis will close
178 preferentially and seismic waves will propagate faster along the same direction (Crampin
179 & Lovell, 1991). To investigate whether the observed H/V ratio anisotropy can be
180 explained by stress-induced microcrack alignment and potentially be used to map the
181 continental stress field with ambient seismic noise, we compare our inferred fast H/V
182 ratio directions with the smoothed stress model of Heidbach et al. (2010). The model was
183 derived based on the compilation of stress-indicators, which primarily consistent of
184 earthquake focal mechanisms and well bore breakouts (Heidbach et al., 2008).
185
186 A clear correlation is observed between the maximum compressive directions of
187 Heidbach et al. (2010) and our inferred fast directions for both the 10 and 16 s period
188 H/V ratios across the contiguous US (Figure 4). For comparison with the stress model
189 we use only the H/V ratio fast directions with anisotropy amplitudes >2%. For locations
190 with a reliable fast direction and where the stress model is available, the fast direction is
191 aligned within 30° of the maximum compressive direction for more than 60% of the

192 locations (Figure 4b,d). This correlation is significant considering that the anisotropy
193 observation and the stress model have a very different lateral resolution and depth
194 sensitivity. Depending on the area, the stress model has a lateral resolution ranging
195 between 100 and 1000 km (Heidbach et al., 2010) where the resolution of the anisotropy
196 measurements is ~ 200 km everywhere due to the 100 km radius station averaging
197 performed. Strong correlations of the two directions are observed in areas such as the
198 Great Basin, Rocky Mountains, and Appalachian Ranges. Weak correlation areas, on the
199 other hand, are relatively scattered and potentially due to resolution mismatch.
200
201 The 180° periodicity of directionally dependent H/V ratio measurements along with
202 correlations between the inferred anisotropy pattern and major geological features and an
203 independently derived stress model demonstrate the utility of measuring H/V anisotropy
204 for studying the upper crust. The 3D anisotropic structure of the lithosphere could be
205 resolved over a broader depth interval by exploiting the complementary sensitivities of
206 the H/V ratio and traditional measurements of anisotropic Rayleigh wave phase velocities
207 (e.g., Lin et al., 2011). Investigations of upper crustal anisotropy where the structural
208 fabric and maximum compressive stress are not aligned will help determine the dominant
209 factor controlling shallow crustal anisotropy. Alaska, for example, with major mountain
210 ranges perpendicular to the maximum compressive stress direction, is an ideal area and
211 will soon be covered by the ongoing USArray deployment. Our present results spanning
212 most of the contiguous US suggest that H/V ratio anisotropy is strongly influenced by the
213 direction of maximum compressive stress in the shallow crust.
214
215 **Acknowledgements**

Instruments (data) used in this study were made available through EarthScope (EAR-0323309), supported by the National Science Foundation. The facilities of the IRIS Data Management System (EAR-0552316) were used to access the waveform and metadata required in this study. F Lin acknowledges the support from University of Utah and a grant from the US National Science Foundation, CyberSEES-1442665, for this research.

References

Aster, R. C., and P. M. Shearer (1992), Initial shear wave particle motions and stress constraints at the Anza Siesmic Network, *Geophys. J. Int.,* **108**, 740–748, doi:10.1111/j.1365-246X.1992.tb03465.x

Bensen, G.D., M.H. Ritzwoller, M.P. Barmin, A.L. Levshin, F. Lin, M.P. Moschetti, N.M. Shapiro, and Y. Yang (2007), Processing seismic ambient noise data to obtain reliable broad-band surface wave dispersion measurements, *Geophys. J. Int.,* **169**, 1239-1260, doi: 10.1111/j.1365-246X.2007.03374.x.

Bonnefoy-Claudet, S., F. Cotton, and P.-Y. Bard (2006), The nature of the seismic noise wave field and its implication for site effects studies: A literature review, *Earth Sci. Rev*., **79**(3–4), 205–227.

Boness, N. L., and M. D. Zoback (2006), A multiscale study of the mechan- isms controlling shear velocity anisotropy in the San Andreas Fault Observatory at Depth, Geophysics, 71(5), doi:10.1190/1.2231107.

Boore, D., and M. Nafi Toksöz (1969), Rayleigh wave particle motion and crustal

238 structure, *Bull. Seism. Soc. Am.*, **59**, 331–346.

239 Crampin, S. (1978), Siesmic-wave propagation through a cracked solid: Polarization as a

240 possible dilatancy diagnostic, *Geophys. J. R. Astron. Soc.,* **53**, 467–496.

241 Crampin, S., and J. H. Lovell (1991), A decade of shear-wave splitting in the Earth's

242 crust: What does it mean? What use can we make of it? And what should we do next?,

243 *Geophys. J. Int.,* **107**, 387–407

244 Crampin, S. (1994), The fracture criticality of crustal rocks, *Geophys. J. Int.*, **118**, 428–

245 438, doi: 10.1111/j.1365-246X.1994.tb03974.x.

246 Flesch, L. M., W. E. Holt, A. J. Haines, and B. Shen-Tu (2000), Dynamics of the Pacific-

247 North American plate boundary in the western United States, *Science*, **834**, 834–836,

248 doi:10.1126/science.287.5454.834.

249 Gerst A., & M.K. Savage (2004), Seismic anisotropy beneath Ruapehu volcano: A

250 possible eruption forecasting tool, *Science*, **306**(5701),1543-1547.

251 Heidbach, O., M. Tingay, A. Barth, J. Reinecker, D. Kurfeß, and B. Müller (2008), The

252 World Stress Map database release 2008 doi:10.1594/GFZ.WSM.Rel2008, accessed at

253 http://dc-app3-14.gfz-potsdam.de/pub/stress_maps/stress_maps.html

254 Heidbach, O., M. Tingay, A. Barth, J. Reinecker, D. Kurfeß, and B. Müller (2010),

255 Global crustal stress pattern based on the World Stress Map database release 2008,

256 *Tectonophysic*s, **462**, doi:10.1016/j.tecto.2009.1007.1023

257 Hinze, W. J., D. J. Allen, A. J. Fox, D. Sunwood, T. Woelk, and A. G. Green (1992),
258 Geophysical investigations and crustal structure of the North American Midcontinent Rift
259 system, *Tectonophysics*, **213**(1–2), 17–32, doi:10.1016/0040-1951(92)90248-5.

260 Jones, C. H., J. Unruh, and L. J. Sonder (1996), The role of gravitational potential energy
261 in active deformation in the southwestern United States, *Nature*, **381**, 37–41.

262 Kern, H., and H.-R. Wenk (1990), Fabric-related velocity anisotropy and shear wave
263 splitting in rocks from the Santa Rosa Mylonite Zone, California, *J. Geophys. Res.,* **95**,
264 11,213–11,223, doi:10.1029/JB095iB07p11213.

265 Laske, G., and G. Masters (1997), A global digital map of sediment thickness, *EOS*
266 *Trans. AGU*, **78**, 483.

267 Lin, F., M.P. Moschetti, and M.H. Ritzwoller (2008), Surface wave tomography of the
268 western United States from ambient seismic noise: Rayleigh and Love wave phase
269 velocity maps, *Geophys. J. Int.,* **173**, 281–198, doi:10.1111/j.1365-246X.2008.03720.x.

270 Lin, F.-C., M.H. Ritzwoller, and R. Snieder (2009), Eikonal Tomography: Surface wave
271 tomography by phase-front tracking across a regional broad-band seismic array, *Geophys.*
272 *J. Int*., **177**, 1091–1110, doi: 10.1111/j.1365-246X.2009.04105.x.

273 Lin, F.C., M.H. Ritzwoller, Y. Yang, M.P.Moschetti, and M.J. Fouch (2011), Complex
274 and variable crustal and uppermost mantle seismic anisotropy in the western United
275 States, *Nature Geoscience*, **4**, 55-61, doi:10.1038/ngeo1036.

276 Lin, F.-C.,B. Schmandt, and V.C. Tsai (2012), Joint inversion of Rayleigh wave phase
277 velocity and ellipticity using USArray: constraining velocity and density structure in the
278 upper crust, *Geophys. Res. Letts*., **39**, L12303, doi:10.1029/2012GL052196.

279 Lin, F.C.,D. Li, R. W. Clayton, and D. Hollis (2013), High-resolution 3D shallow crustal
280 structure in Long Beach, California: Application of ambient noise tomography on a dense
281 seismic array, *Geophysics*, **78**(4), Q45-Q56,doi:10.1190/geo2012-0453.1, 2013

282 Lin, F.C., V.C. Tsai, and B. Schmandt (2014), 3-D crustal structure of the western United
283 States: application of Rayleigh-wave ellipticity extracted from noise cross-correlations,
284 *Geophys. J. Int*, **198**(2), 656-670, doi: 10.1093/gji/ggu160.

285 Mordret, A., N. M. Shapiro, S. Singh, P. Roux, J.-P. Montagner, and O. I.
286 Barkved (2013), Azimuthal anisotropy at Valhall: The Helmholtz equation
287 approach, *Geophys. Res. Lett.*, **40**, 2636–2641, doi:10.1002/grl.50447**.**

288 Savage, M. K. (1999), Seismic anisotropy and mantle deformation: What have we
289 learned from shear wave splitting?, *Rev. Geophys.,* **37**(1), 65–106,
290 doi:10.1029/98RG02075.

291 Shen, W., M.H. Ritzwoller, and V. Schulte-Pelkum (2013), Crustal and uppermost
292 mantle structure in the central US encompassing the Midcontinent Rift, *J. Geophys. Res.*,
293 **118**, 4325-4344, doi:10.1002/jgrb.50321.

294 Sherrington, H. F., G. Zandt, and A. Frederiksen (2004), Crustal fabric in the Tibetan
295 Plateau based on waveform inversions for seismic anisotropy parameters, *J. Geophys.*
296 *Res*., **109**, B02312, doi:10.1029/2002JB002345.

297 Smith, M.L. & Dahlen, F.A. (1973), Azimuthal dependence of Love and Rayleigh-wave
298 propagation in a slightly anisotropic medium, *J. Geophys. Res*., **78**, 3321–3333.

299

300 Smith, Robert B., and Marc L. Sbar (1974), Contemporary tectonics and seismicity of the
301 western United States with emphasis on the Intermountain Seismic Belt." *Geological*
302 *Society of America Bulletin* 85.8 (197), 1205-1218.
303

304 Tanimoto, T., and L. Rivera (2008), The ZH ratio method for long-period seismic data:
305 Sensitivity kernels and observational techniques, *Geophys. J. Int*., **172**, 187–198.
306 doi: 10.1111/j.1365-246X.2007.03609.x.

307 Tanimoto T., Yano T., Hakamata T. (2012), An approach to improve Rayleigh-wave
308 ellipticity estimates from seismic noise: application to the Los Angeles Basin. *Geophys.*
309 *J. Int*., **190**, 1097-1110.

310 Whitmeyer, S. J., and K. E. Karlstrom (2007), Tectonic model for the Proterozoic growth
311 of North America, *Geosphere*, **3**(4), 220–259, doi:10.1130/ges00055.1.

312 Yang, Z., A. Sheehan, and P. Shearer (2011), Stress‐induced upper crustal anisotropy in
313 southern California, *J. Geophys. Res.,* **116,** B02302, doi:10.1029/2010JB007655.

314 Yano, T., T. Tanimoto, and L. Rivera (2009), The ZH ratio method for long-period
315 seismic data: Inversion for *S*-wave velocity structure, *Geophys. J. Int*., **179**, 413–424.
316 doi: 10.1111/j.1365-246X.2009.04293.x.

317

318 **Figure Captions**

319 Figure 1. (a) The 10 s Rayleigh wave H/V ratio observed across USArray. The letters a,
320 b, and c indicate the example locations used in Figure 2. The red contours denote the
321 tectonic boundaries in the western US. The blue contour denotes the approximate
322 locations of the Midcontinent Rift and the Precambrian Rift Margins in the eastern US
323 (Whitmeyer & Karlstrom, 2007). Several states mentioned in the text are also identified.
324 UT: Utah; NE: Nebraska; OK: Oklahoma; MN: Minnesota; IA: Iowa; AL: Alabama; VA:
325 Virginia. (b) The depth sensitivities of the 10 s H/V ratio to Vs, Vp, and density (ρ). (c)-
326 (d) Same as (a)-(b) but for the 16 s H/V ratio. GB: Great Basin; CP: Colorado Plateau;
327 RM: Rocky Mountains; IP: Interior Plain Province; EM: Mississippi Embayment; LH:
328 Laurentian Highlands; OH: Ouachita-Ozark Interior Highlands; AH: Appalachian
329 Highlands.

330 Figure 2. (a)-(c) Examples of 10 s directionally dependent Rayleigh wave H/V ratio
331 perturbations at the locations denoted in Figure 1a. The red bars represent the mean
332 perturbations and their uncertainties in each 20° azimuthal bin relative to the isotropic
333 H/V ratio. For each case, the solid green line is the best fit of the 180° periodicity
334 azimuthal variation. The high H/V ratio direction and the variation amplitude of the fit
335 are also shown. (d)-(f) Same as (a)-(c) but for the 16 s period.

336 Figure 3. (a) The azimuthal anisotropy of the 10 s period Rayleigh wave H/V ratio. The
337 red bars indicate the low H/V ratio directions (or the inferred upper crustal fast
338 directions). The lengths of the bars are proportional to the peak-to-peak amplitudes,
339 which are also shown by the background color. (b) Same as (a) but for the 16 s period.

Figure 4. The comparison between the maximum compressive stress directions and the inferred upper crustal fast directions. (a) The colored bars show the maximum compressive stress axes modeled by Heidbach et al. (2010). The blue, red, and black colors identify angle differences between the stress direction and the fast direction inferred by 10 s H/V ratio anisotropy: Blue: 0°-30°, Red: 30°-60°, Black: 60°-90°. The green color identifies locations with observed anisotropy amplitudes smaller than 2%, where the fast directions cannot be robustly determined. (b) The distribution of angle differences between the compressive stress direction and fast direction inferred by 10 s H/V ratio anisotropy. (c)-(d) Same as (a)-(b) but for 16 s H/V ratio anisotropy.

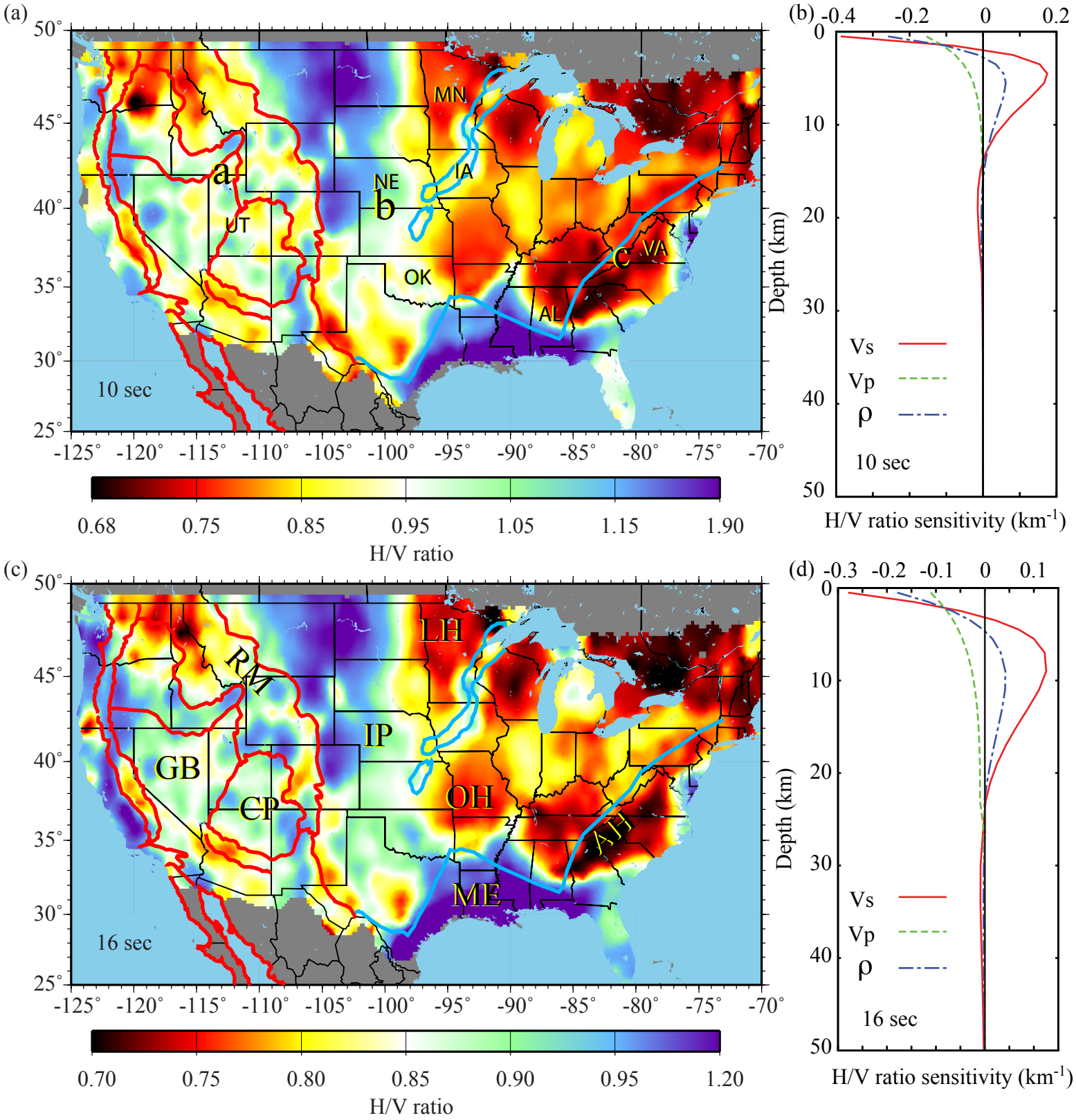
(a)
(b)
(c)
(d)
MN
IA
NE
UT
OK
VA
AL
a
b
c
10 sec
Vs
Vp
ρ
Depth (km)
H/V ratio sensitivity (km-1)
H/V ratio
LH
RM
IP
GB
CP
OH
ATH
ME
16 sec

Figure 1

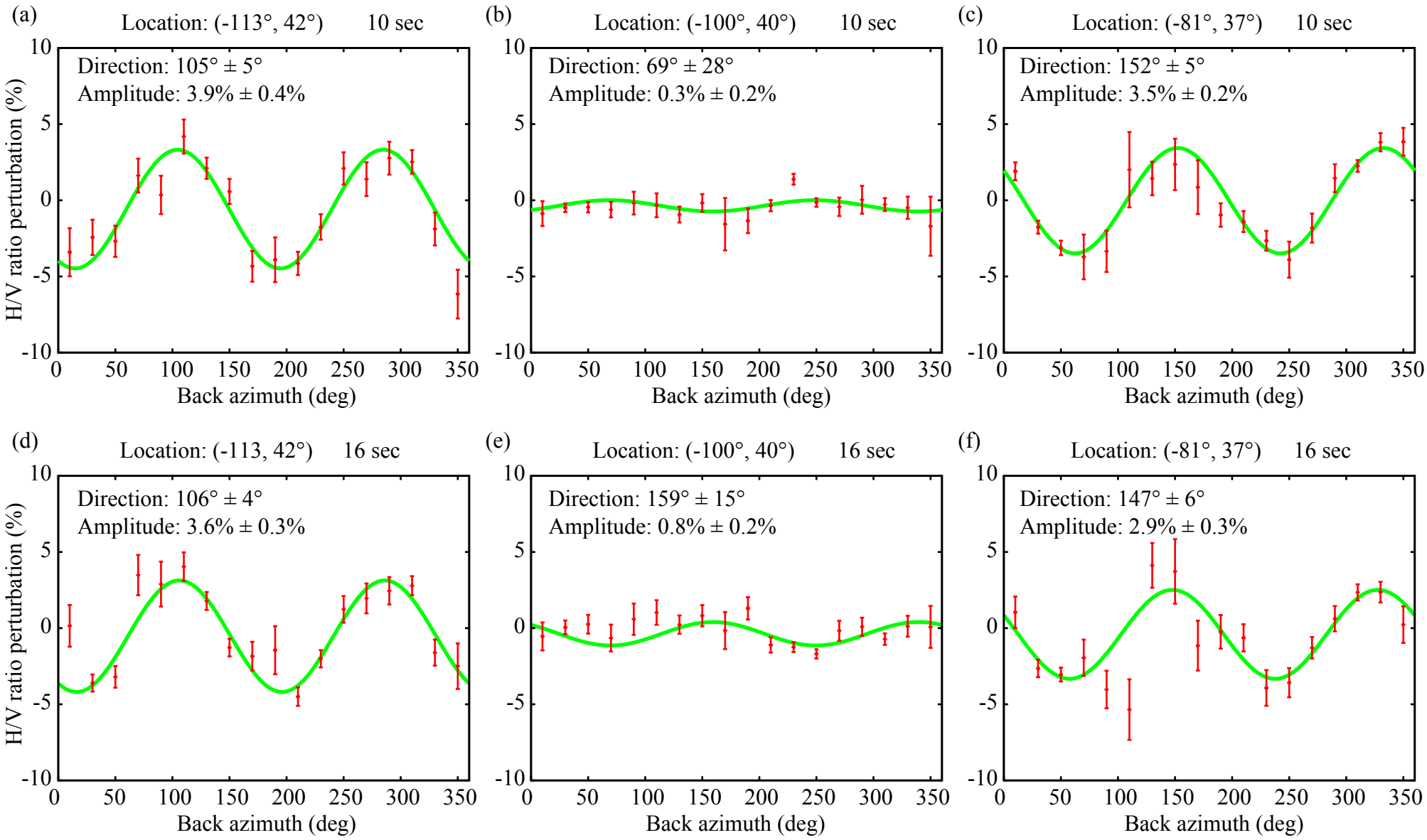
(a)
Location: (-113°, 42°) 10 sec
Direction: 105° ± 5°
Amplitude: 3.9% ± 0.4%
(b)
Location: (-100°, 40°) 10 sec
Direction: 69° ± 28°
Amplitude: 0.3% ± 0.2%
(c)
Location: (-81°, 37°) 10 sec
Direction: 152° ± 5°
Amplitude: 3.5% ± 0.2%
(d)
Location: (-113, 42°) 16 sec
Direction: 106° ± 4°
Amplitude: 3.6% ± 0.3%
(e)
Location: (-100°, 40°) 16 sec
Direction: 159° ± 15°
Amplitude: 0.8% ± 0.2%
(f)
Location: (-81°, 37°) 16 sec
Direction: 147° ± 6°
Amplitude: 2.9% ± 0.3%
H/V ratio perturbation (%)
Back azimuth (deg)
10
5
0
-5
-10
0
50
100
150
200
250
300
350

Figure 2

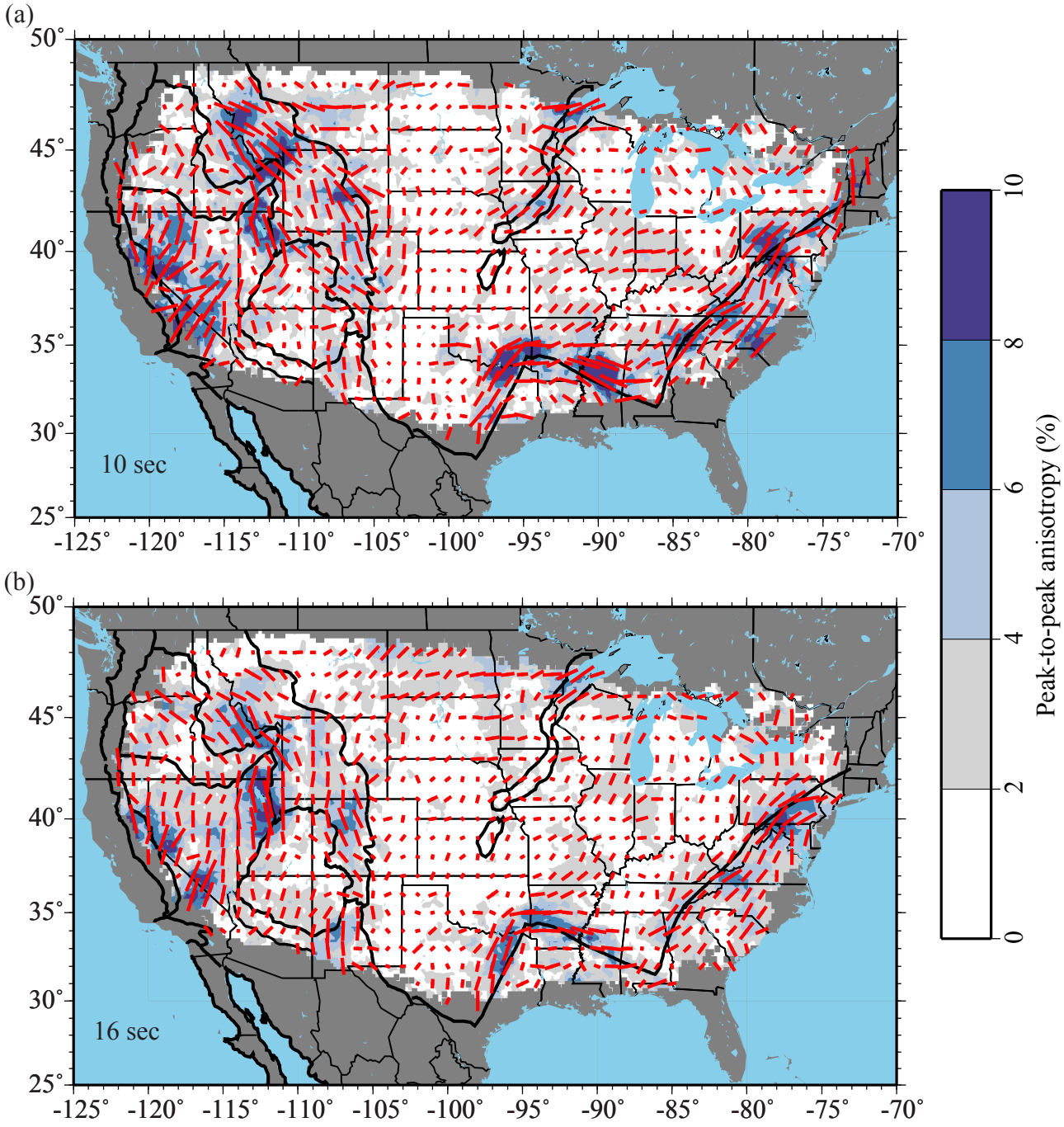
(a)
50°
45°
40°
35°
30°
25°
10 sec
-125° -120° -115° -110° -105° -100° -95° -90° -85° -80° -75° -70°
(b)
50°
45°
40°
35°
30°
25°
16 sec
-125° -120° -115° -110° -105° -100° -95° -90° -85° -80° -75° -70°
0
2
4
6
8
10
Peak-to-peak anisotropy (%)

Figure 3

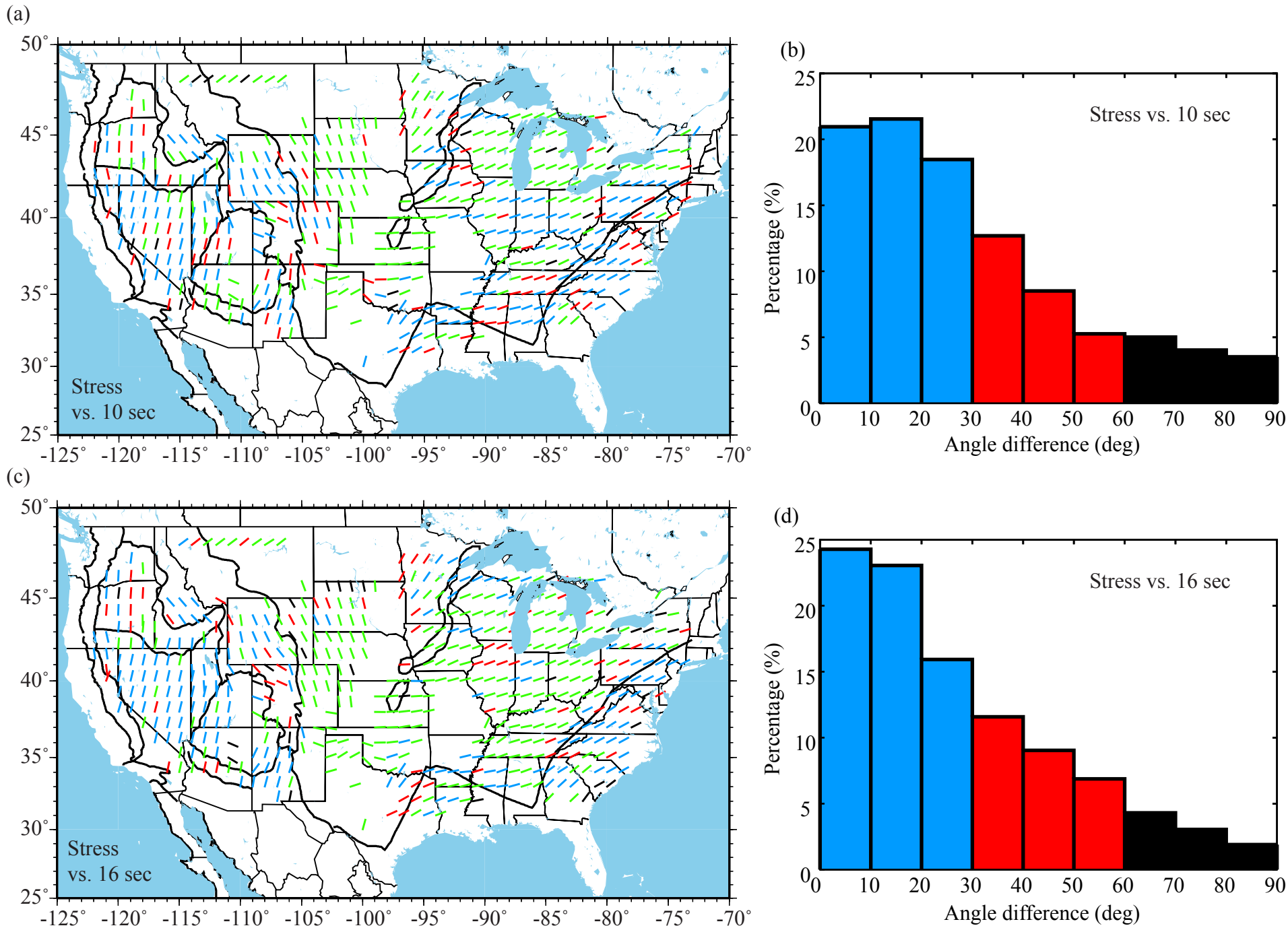
(a)
Stress
vs. 10 sec
(b)
Stress vs. 10 sec
Percentage (%)
Angle difference (deg)
(c)
Stress
vs. 16 sec
(d)
Stress vs. 16 sec
Percentage (%)
Angle difference (deg)

Figure 4